European Journal of Radiology 112 (2019) 52–58

Contents lists available at ScienceDirect

European Journal of Radiology

journal homepage: www.elsevier.com/locate/ejrad

Research article

Fast isotropic volumetric magnetic resonance imaging of the ankle: Acceleration of the three-dimensional fast spin echo sequence using compressed sensing combined with parallel imaging

Jisook Yi[1], Young Han Lee*, Seok Hahn[1], Salman S. Albakheet, Ho-Taek Song, Jin-Suck Suh

Department of Radiology, Research Institute of Radiological Science, YUHS-KRIBB Medical Convergence Research Institute, and Severance Biomedical Science Institute, Yonsei University College of Medicine, Seoul, Republic of Korea

ARTICLE INFO

Keywords:
Compressed sensing
MR
Ankle

ABSTRACT

Objectives: To investigate the feasibility of three-dimensional fast spin echo (3D-FSE) imaging with compressed sensing (CS) and parallel imaging (PI) compared to 3D-FSE imaging with only PI in evaluating ankle joint pathologies.

Materials and methods: Twenty consecutive patients underwent ankle magnetic resonance imaging (MRI), including acquisition of image sets of 2D-FSE sequences, and 3D-FSE sequences without and with CS, between June 2016 and November 2017. Three MR image sets were independently rated by two radiologists for the presence/absence of ankle pathology. Quantitative image similarity and subjective image quality were evaluated using 3D-FSE images without CS and those with CS-PI. Inter-sequence agreement between 3D-FSE sequences without CS and with CS-PI in both readers was evaluated.

Results: Interobserver agreements were nearly perfect for sprain of the anterior talofibular ligament (ATFL, $\kappa = 0.77$), osteochondral lesion of the talus (OLT, $\kappa = 0.76$-0.88), osteochondral lesion of the distal tibia (OLTi, $\kappa = 0.74$) and os subfibulare (OSF, $\kappa = 0.62$-0.64). The structural similarity index (mean, 0.996; range, 0.990-0.997) between the 3D-FSE sequences without CS and with CS-PI was acceptable. There was no significant difference in subjective image quality between the two imaging sequences (ATFL, $p = 0.317$; bone marrow, $p = 0.083$; cartilage, $p = 1.000$, tendon, $p = 1.000$). Intersequence agreement between the 3D-FSE sequences with and without CS was nearly perfect (ATFL and OLTi, $\kappa = 1.00$; OLT, $\kappa = 0.87$-0.96; OSF, $\kappa = 0.62$-0.64) in both readers.

Conclusions: Isotropic 3D-FSE ankle MRI with CS provides acceptable diagnostic performance with reduced scan time. Compressed sensing-related artifacts could be minimized with CS reconstruction enhancement, allowing for better image quality for evaluating ankle joint pathologies.

1. Introduction

Comprehensive intra-articular and extra-articular evaluation of the ankle requires radiologic examinations to visualize the internal structures of joints, ligaments, tendons, cartilages, and the bone marrow [1]. Sprain of the ankle joint is one of the most common sports injuries, which accounts for 10–15% of all sports injuries [2], and most cases of acute sprain of the ankle joint heals with conservative treatment; however, a significant number of cases do progress to joint instability, limited range of motion, and osteoarthritis [3,4]. Magnetic resonance imaging (MRI) is the imaging modality of choice because of the following reasons: superior soft tissue contrast, high spatial resolution, multiplanar imaging capability, lack of ionizing radiation, and capability of gadolinium contrast imaging [5–7]. Utilization of MRI for the ankle can be maximized by using the multiplanar imaging of the axial, coronal, and sagittal planes, which facilitates the visualization of the small complex structures of the ankle. Also, detailed high-spatial resolution MRI is required in ankle and foot imaging, because MRI evaluation of the ankle and foot is often a complex task given the small size of anatomic structures and complex multi-articulated anatomic structures. For this detailed MRI evaluation, three-dimensional (3D) imaging with high spatial resolution, thin slice imaging, and isovoxel imaging with MPR capability are required.

The isovoxel three dimensional (3D)-fast spin echo (FSE) sequence

* Corresponding author at: Department of Radiology, Yonsei University College of Medicine, 50-1 Yonsei-ro, Seodaemun-gu, Seoul 03722, Republic of Korea.
E-mail address: radiologie@gmail.com (Y.H. Lee).
[1] Present address: Department of Radiology, Inje University College of Medicine, Haeundae Paik Hospital, Busan, Republic of Korea.

https://doi.org/10.1016/j.ejrad.2019.01.009
Received 28 September 2018; Received in revised form 5 January 2019; Accepted 8 January 2019

of ankle MRI has the capabilities of acquiring thin-sliced sections and performing MPR without any loss of spatial resolution, and has shown to be comparable to or even better than the 2D FSE sequence, which is widely used as the routine MRI sequence for evaluating ankle pathologies [8–12]. To obtain isovoxel sequence of ankle joint, many thin sliced sections are required, and moreover over coverage of the ankle joint is required to minimize wraparound artifacts. And those result in long scan time. The long scan time of 3D-FSE imaging is a major hurdle to the use of the isotropic high-spatial resolution 3D-FSE sequence, as it could cause motion artifacts and discomfort to patients. Parallel imaging (PI) acceleration techniques have been used to overcome the long scan time of the 3D-FSE sequence [13], and even widely used 3D FSE techniques such as the Cube®, VISTA®, and SPACE® have adopted parallel imaging for clinically feasible scan times [6,7,14].

Recently, fast MR imaging has been accelerated with the compressed sensing (CS) technique. The CS technique is a method to accelerate MR acquisition by acquiring undersampling κ-space data [15]. In several recent studies, the CS technique has been applied to the 3D sequence of MRI, which helped reduce the scan time while showing minimal effect on image quality [15–19]. Several investigations have used the combination of CS and PI to reduce the scan time; these studies have concluded that the images obtained were of a comparable or better quality than that of the images obtained using only PI [16–18]. To the best of our knowledge, there has been no published study utilizing 3D-FSE MRI with CS-PI for the ankle joint. The purpose of the present study was to investigate the feasibility of 3D-FSE imaging with CS-PI compared to 3D-FSE imaging with only PI in evaluating ankle joint pathologies.

2. Subjects and methods

2.1. Study population

This study was approved by the relevant institutional review board. Between June 2016 and November 2017, a total of 121 consecutive patients with a complaint of ankle pain had undergone ankle MRI. Exclusion criteria were pediatric patients (age under 18 years, n = 17), patients with infection (n = 4), patients with a tumor (n = 8), those who had undergone ankle surgery previously (n = 6), and those for whom 3D-FSE data were not available (n = 66). In total, 20 patients, including 12 men (aged 20—61 years; mean age, 38.6 years) and 8 women (aged 21—67 years; mean age, 45.1 years) were eligible for enrollment in this study.

2.2. Imaging study

MRI was performed using a 3.0-T magnetic resonance system (Discovery 750, GE Healthcare, Waukesha, WI, USA) with a 16-channel GEM Flex-medium flexible coil (NeoCoil, Pewaukee, WI, USA). 2D-FSE images for comparison with reformats of the 3D-FSE images were acquired in the axial, sagittal, and coronal planes. Images of 3D-FSE with only PI and 3D-FSE with CS-PI were obtained from the sagittal plane. Table 1 shows the imaging protocol parameters. Autocalibrating Reconstruction for Cartesian sampling (ARC™, GE Healthcare) acceleration factor of 2 was used in both phase and slice directions, and the intermediate weighted (IW) 3D-FSE with CS-PI sequence was obtained using a 1.5 k-space undersampling CS factor [17,20]: IW 3D-FSE with only PI was 2 × 2, and IW 3D-FSE with CS-PI was 2 × 2 x 1.5.

2.3. Quantitative image analysis

For quantitative image comparison, structural similarity (SSIM) index, which compares pixel intensities normalized for luminance and contrast, was calculated to compare objective image quality between IW 3D-FSE sequences with and without CS [21]. The central single slice of IW 3D-FSE MR images with and without CS was selected by a radiologist (J.Y). Furthermore, image datasets in Digital imaging and Communications in Medicine format were analyzed using MATLAB (Math Works, Natick, MA, USA). An SSIM index of 1 represents perfect identity, and it decreases as the images differ [22].

2.4. Qualitative image analysis

Image analysis was performed independently and in random order by two fellowship-trained musculoskeletal radiologists (with 7 and 11 years of clinical experience) who were blinded to the electronic medical records of the patients, including the radiology report and the final diagnosis. The images were digitally assessed with a commercially available PACS workstation (Centricity® Radiology RA1000; GE Healthcare, Barrington, IL, USA). To avoid recall bias, the radiologists evaluated the three image sets with at least a 2-week interval between sessions of evaluation. Multiplanar reformation of the IW 3D-FSE images was performed using the Aquarius iNtuition software package (ver. 4.4.11; TeraRecon, Inc., San Mateo, CA, USA) [8]. The radiologists assessed the 2D FSE, 3D IW-FSE without CS, and 3D IW-FSE with CS sequences to rate the presence of anterior talofibular ligament (ATFL) tear, osteochondral lesion of the talus (OLT), osteochondral lesion of the tibia (OLTi), and Os subfibulare (OSF).

An ATFL tear was defined as complete or partial discontinuity, thickening, thinning, wavy contour, and increased signal intensity on the ATFL [1]. The areas of the talar trochlear cartilage and the articular surface of the distal tibia were divided into 6 compartments: anteromedial, anterolateral, mid medial, mid lateral, posteromedial, and posterolateral area. An OLT was defined as increased signal intensity, surface irregularity, detachment of cartilage from the talar trochlea, with or without subchondral cyst/bone marrow edema [1]. In addition, the presence or absence of OLT in each area was rated. OLTi was also defined as increased signal intensity, surface irregularity, detachment of cartilage from the distal tibia, with or without subchondral cyst/bone marrow edema. The presence or absence of OLTi in each area was rated. The presence or absence of OSF was evaluated regardless of ATFL tear.

Two radiologists rated the subjective image quality of IW 3D-FSE without CS and with CS sequences by consensus using a 4-point scale: clarity of ATFL, bone marrow, cartilage, and tendon (4 = excellent: optimal diagnostic value and clearly shows the structure, 3 = good: good for the majority of diagnoses, 2 = acceptable for the majority of diagnoses and the evaluation of the structure was somewhat limited, 1 = poor: poor for the majority of diagnoses and the evaluation of the structure was substantially limited).

2.5. Statistical analysis

Wilcoxon's signed-rank test was used to compare the subjective image quality scores between IW 3D-FSE sequences with and without CS. The interobserver and intersequence agreements were calculated using Cohen's kappa statistics. All statistical analyses were performed using SPSS software (version 23; SPSS Inc., Armonk, NY, USA). *P* values < 0.05 were deemed to indicate statistically significant differences.

3. Results

The mean SSIM index value between the IW 3D-FSE sequences with and without CS was 0.996 (range, 0.990-0.997), which is acceptable [22]. The interobserver agreement was substantial to nearly perfect for ATFL (κ = 0.77 for all sequences), OLT (2D-FSE, κ = 0.76; IW 3D-FSE with only PI, κ = 0.88; IW 3D-FSE with CS-PI, κ = 0.80), OLTi (κ = 0.74 for all sequences), and OSF (2D-FSE and IW 3D-FSE with only PI, κ = 0.62; IW 3D-FSE with CS-PI, κ = 0.64) via 2D-FSE, IW 3D-FSE with only PI, and IW 3D-FSE with CS-PI sequences (Figs. 1 and 2). Two of the IW 3D-FSE sequences showed better interobserver agreement in evaluating OLT. The intersequence agreement between the IW 3D-FSE

Table 1
Magnetic resonance imaging parameters.

Parameters	2D-FSE sequence			IW 3D-FSE with only PI sequence	IW 3D-FSE with CS-PI sequence
	IW axial	T2-W FS coronal	T1-W sagittal		
Repetition time (ms)	4004.0	3912.0	681.0	1300.0	1300.0
Echo time (ms)	24.3	62.8	12.0	36.7	36.7
Field of view (cm)	12	14	15	16	16
Section thickness/gap (mm)	3/0.3	3/0.3	3/0.3	0.5/0	0.5/0
Acquisition matrix	512 × 320	352 × 288	512 × 352	320 × 320	320 × 320
Reconstructed matrix (mm)	512 × 512	512 × 512	512 × 512	512 × 512	512 × 512
Echo train length	3	12	3	38	38
Number of excitations	1	1	1	1	1
Fat suppression	No	Yes	No	Yes	Yes
Arc acceleration factor in the phase and slice direction				2 × 2	2 × 2
CS acceleration factor					1.5
Acquisition time	4 min	4 min 2 sec	4 min 34 sec	7 min 47 sec	5 min 20 sec

2D = two-dimensional, FSE = fast spin-echo, IW = intermediate weighted, 3D = three-dimensional, PI = parallel imaging, CS-PI = compressed sensing combined with parallel imaging, Arc = Autocalibrating Reconstruction for Cartesian sampling.

with only PI and IW 3D-FSE with CS-PI sequences was substantial for OSF (reader 1, κ = 0.62; reader 2, κ = 0.64), and almost perfect for ATFL (reader 1, κ = 1.00; reader 2, κ = 1.00), OLT (reader 1, κ = 0.96; reader 2, κ = 0.87), OLTi (reader 1, κ = 1.00; reader 2, κ = 1.00) in both of readers. Most of the ankle pathologies seemed similar in the IW 3D-FSE with only PI and IW 3D-FSE with CS-PI sequences (Figs. 1 and 2). There was no significant difference in the subjective image quality which reached consensus by both readers between the IW 3D-FSE with only PI and IW 3D-FSE with CS-PI sequences (ATFL, $p = 0.317$; bone marrow, $p = 0.083$; cartilage, $p = 1.000$; tendon, $p = 1.000$).

4. Discussion

Imaging speed and scan time have been an issue for application of MRI in clinical practice [23–28]. Compressed sensing is a fast MR imaging technique, which is based on reconstructing images from undersampling of k-space data [15]. It requires an irregular undersampling pattern that will not cause structured aliasing artifacts in the image domain [15,29]. Then, a nonlinear reconstruction is used to reconstruct the undersampled k-space date [15]. Undersampling phase-encoding lines provide randomness in the phase-encoding direction and it also enables reduction of scan time, which is exactly proportional to the undersampling [15].

In the current study, we implemented CS combined with PI to shorten the scan time of isotropic 3D-FSE imaging of the ankle. In clinical practice, one 3D sequence requiring a scan time of more than 7 min is not an optimal imaging sequence, considering the patients who undergo ankle MRI have ankle pain and that occasionally, ankle swelling needs to be in the MRI bore with an ankle rectangle flexed position. Given that most of patients who undergo MRI after ankle sprain experience pain, and a long scan time would mean that the patient needs to have considerable endurance, sequences with a long scan time are not suitable for clinical practice. The long scan time can be reduced by applying the fast imaging technique with CS acceleration from 7:47 min to 5:20 min, and it would contribute to patient comfort without significantly degrading image quality.

Under-sampled *k* space and CS reconstructions could result in blurry images and cause over-smoothening. In quantitative comparison using SSIM, the average SSIM value was used to assess the overall quantitative image quality of CS, which can be deemed to be acceptable when the value is over 0.950, and in the present study, the result was acceptable (0.996) [22,30]. In addition to this quantitative comparison, we evaluated the subjective image quality of key structures, which should be clearly delineated on MRI, and the radiologists agreed to similar subjective image quality between isotropic 3D with only PI and with CS-PI sequences in evaluating ATFL, the bone marrow, cartilage, and tendon of the ankle without significant artifact in both sequences. The interobserver agreements for ATFL and OSF were nearly the same for the 2D-FSE, isotropic 3D-FSE with only PI and with CS-PI sequences, and these results were similar to those obtained in a previous study [8]. For OLT, two of the isotropic 3D IW-FSE with only PI and with CS-PI sequences showed slightly better interobserver agreement than the 2D-FSE sequence, and this result is also consistent with the findings of a previous study, which showed slightly better interobserver agreement in isotropic 3D-FSE sequence than in 2D-FSE sequence [8]. OLTi is one of the causes of chronic ankle pain. It is not a rare finding on MRI, but it has often been underestimated as a cause of ankle pain [31,32]. Our result shows an interobserver agreement in evaluating osteochondral lesion of the distal tibia that is similar to that of a previous study (κ = 0.73), and none of the lesions were a kissing lesion of the osteochondral lesion of the talus (Figs. 2 and 3) [31,32].

Our study found substantial to almost perfect intersequence agreements between the isotropic 3D IW-FSE with only PI and with CS-PI sequences for both readers in evaluating ankle pathology. This might suggest the feasibility of the CS-PI technique in the isotropic 3D-FSE sequence of ankle MRI in clinical practice. Though there was no statistical significant difference in the evaluation of the image quality of the bone marrow, 3D-FSE with CS-PI images showed a lower score than 3D-FSE with only PI images ($p = 0.083$, 79 versus 76) for the visualization of the bone marrow, which showed more inhomogeneous texture with some artifacts. However, it was sufficient to evaluate bone marrow edema or subchondral cyst and did not affect the interobserver or intersequence agreements for evaluating ankle pathology. Furthermore, this result is consistent with the result of a previous study that evaluated knee joint pathologies, including bone marrow edema, and reported similar interobserver and inter-sequence agreements between 3D-FSE with CS-PI images and 3D-FSE with only PI images [17]. However, CS-related artifacts and the suboptimal image quality of the bone marrow need to be improved. One of the solutions might be development and improvement of compressed sensing reconstructions via deep learning powered imaging reconstructions [33].

In terms of parallel imaging and compressed sensing, the accelerations would depend on the signal-to-noise ratio (SNR) of the acquired image sequence, imaging matrix size, and channel numbers of used radiofrequency coils [29,34]; the original SNR is important because each accelerated acquisition gathers the fraction of the k-space energy of the original; the imaging matrices influence the scope of irregular k-space sampling patterns; the channel numbers of radiofrequency coil affects the extent to which parallel imaging should be combined with compressed sensing [29]. Herein, we used a 16-channel flexed surface coil, which showed more accelerations and SNR than the 8-channel ankle-dedicated volume coil. In addition, the geometry (g)-factor of

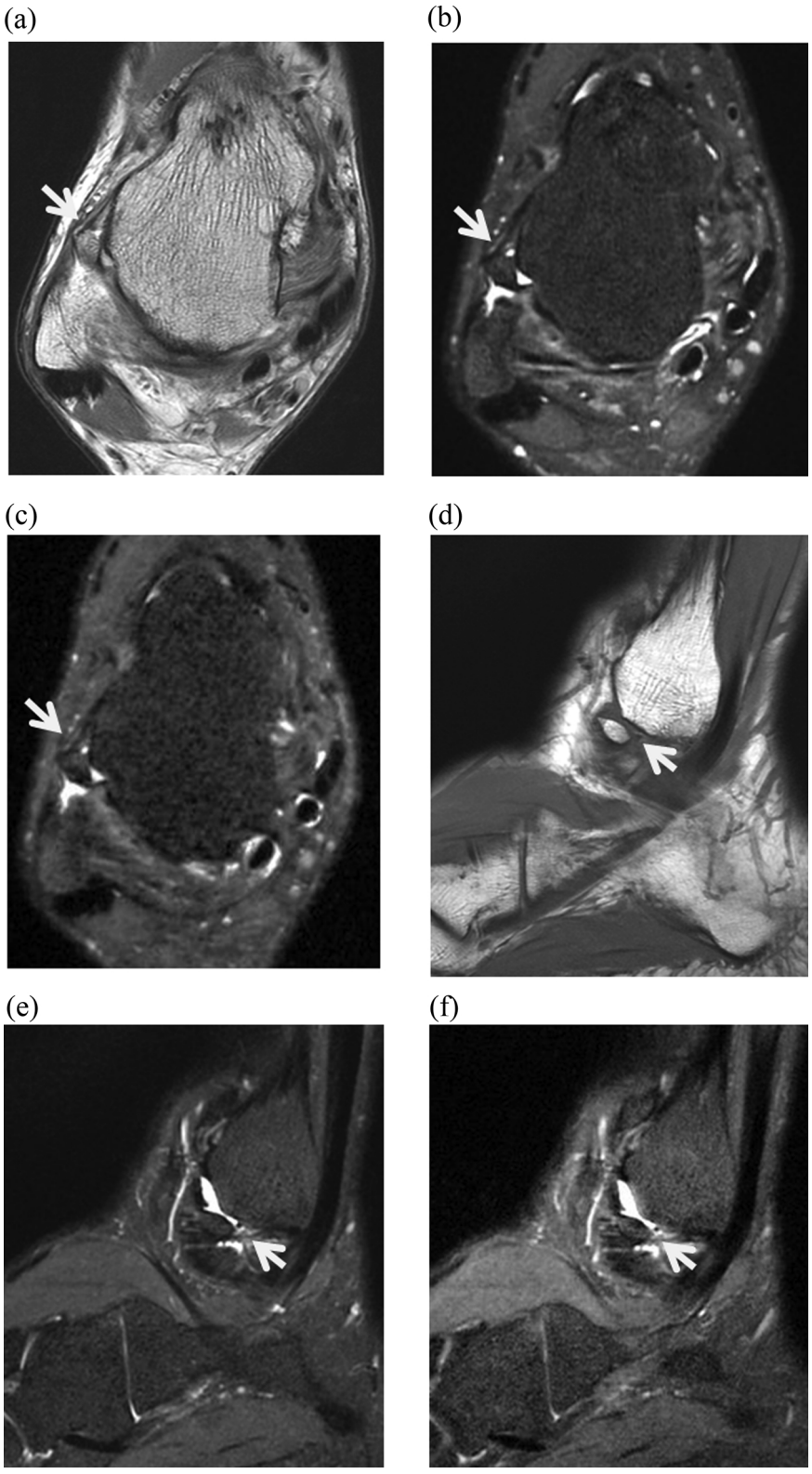

Fig. 1. A 36-year-old man with ankle pain. Axial images of (A) intermediate-weighted (IW) 2 dimensional (2D)-fast spin echo (FSE), (B) IW 3 dimensional (3D)-FSE with parallel imaging (PI) only, and (C) IW 3D-FSE with compressed sening (CS)-PI sequences show similar appearance of anterior talofibular ligament tear and Os subfibulare (arrows). Sagittal images of (D) T1-weighted 2D-FSE, (E) IW 3D-FSE with only PI, and (F) IW 3D-FSE with CS-PI sequences in the same patient show similar appearance of Os subfibulare with displacement (arrows).

radiofrequency coil influences the SNR, which varies according to the spatial position [35,36]. We expect that more CS acceleration could be possible with a newly designed RF coil with higher g-factor and by using a new coil design-optimized 3D FSE CS sequence.

There are some limitations to this study. First, the number of patients was relatively small. This initial study showed the feasibility of the application of CS combined with PI to ankle MRI by comparing with CS-reconstructed images. Second, we did not address the coil

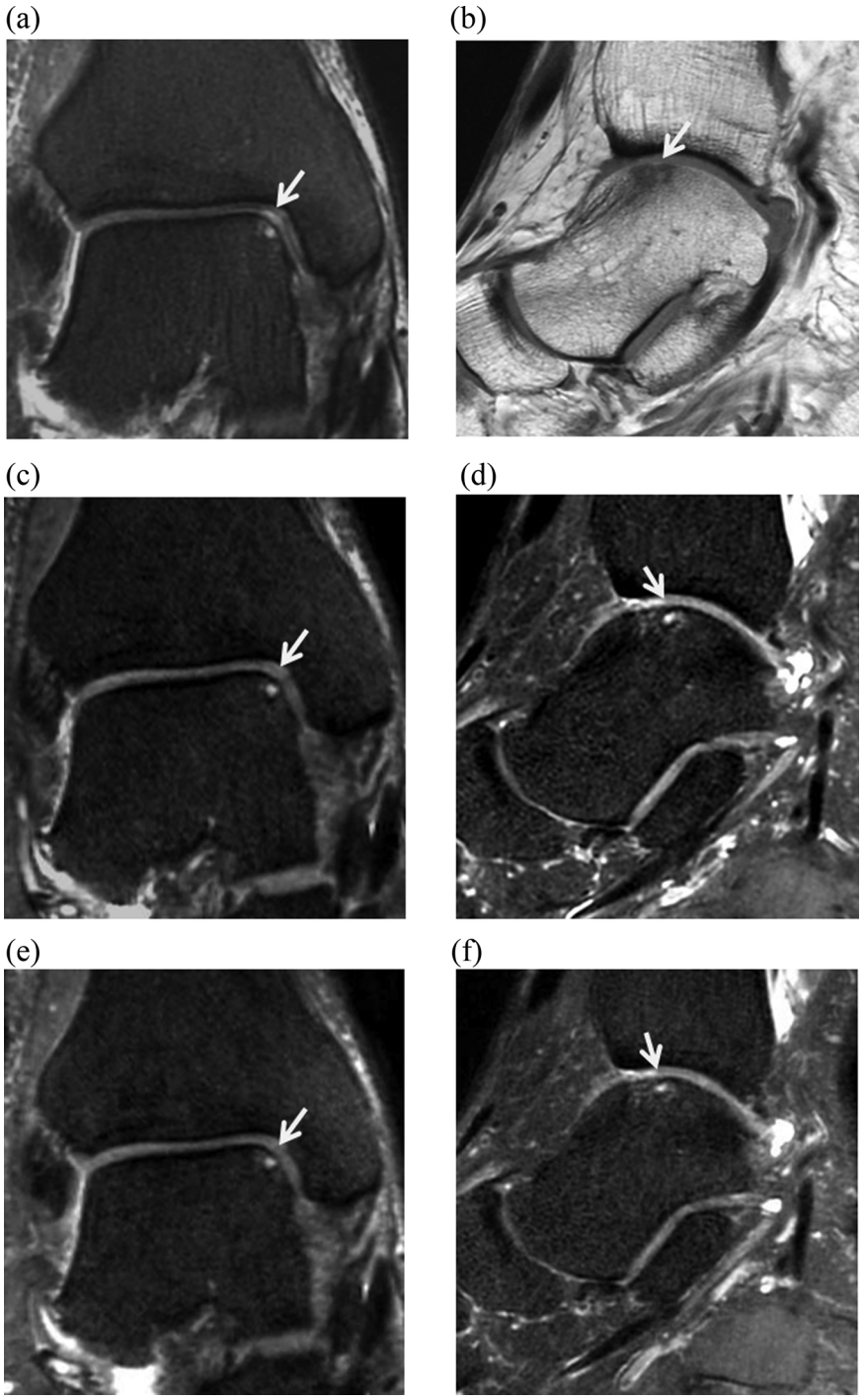

Fig. 2. A 60-year-old man with ankle pain. (A) Coronal 2 dimensional (2D)-fast spin echo (FSE) T2-weighted fat suppressed image shows osteochondral lesion of the talus at the anteromedial area, showing increased signal intensity of the talar cartilage with a subchondral cyst (arrow). (B) Sagittal T1-weighted 2D-FSE image also show osteochonral lesion of the talus with a subchondral cyst. Coronal and sagittal axial images of IW 3 dimensional (3D)-FSE with parallel imaging (PI) only (C, D) and IW 3D-FSE with CS-PI sequences (E, F) show the same appearance of osteochondral lesion of the talus at the anteromedial area.

differences. Image acceleration of CS depends on the number and geometry of radiofrequency coils. We expect that a high number of CS factors can be used in newly designed radiofrequency coils. Third, we compared T2-weighted 2D-FSE coronal image and IW 3D-FSE images with or without CS. It might cause magic angle artifact on IW sequence [37]. But the interobserver agreement for OTL and OLTi in IW 3D-FSE was comparable to 2D-FSE sequence. Fourth, there was no surgical standard that could be correlated with the imaging-based diagnosis. However, the aim of this study was to evaluate the feasibility of the 3D-FSE sequence of the ankle joint with CS and further studies that include a large number of patients with surgical confirmation are needed.

In conclusion, compressed sensing accelerated isotropic 3D-FSE ankle MRI provides acceptable diagnostic performance with reduced scan time. Compressed sensing-related artifacts could be minimized with CS reconstruction enhancement, allowing for better image quality for evaluation of ankle joint pathology.

Declarations of interest

None.

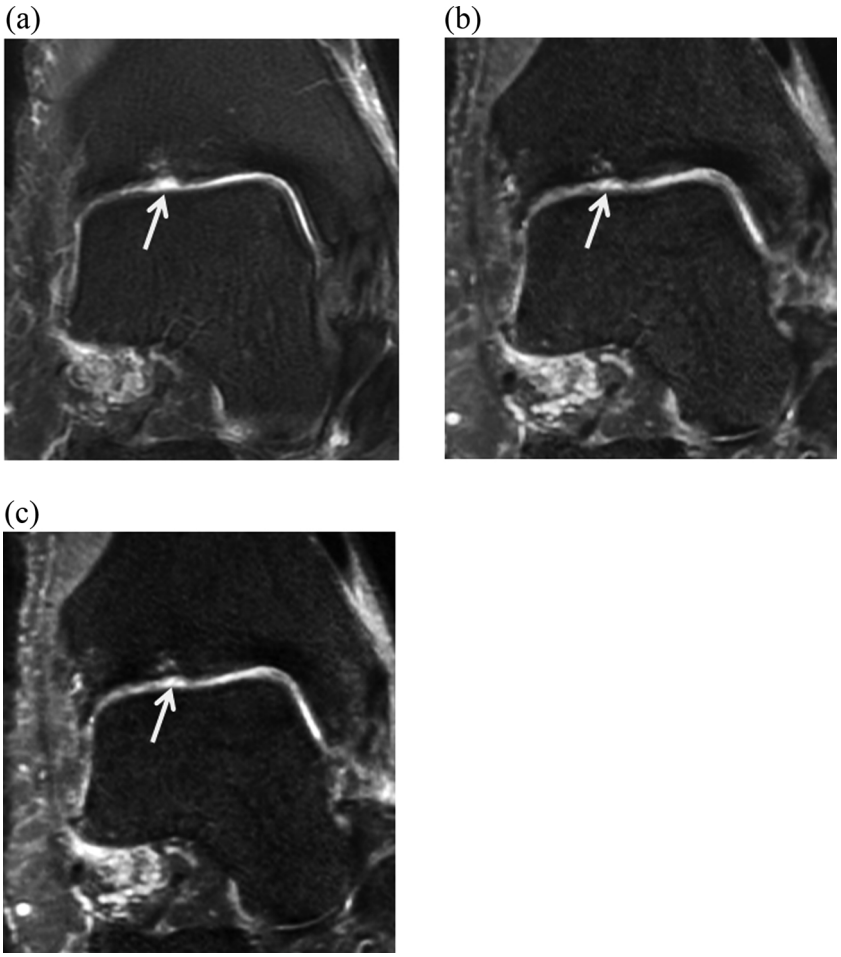

Fig. 3. A 60-year-old man with ankle pain (the same patient described in Fig. 2). (A) Coronal 2 dimensional (2D)-fast spin echo (FSE) T2-weighted fat suppressed image shows osteochondral lesion of the distal tibia at the anterolateral area, showing a focal defect of a cartilage with a subchondral cyst (arrow). Coronal images of IW 3 dimensional (3D)-FSE with parallel imaging (PI) only (B) and IW 3D-FSE with CS-PI sequences (C) show the same appearance of osteochondral lesion of the distal tibia at the anterolateral area.

IRB statement

The institutional review board of our hospital approved this single-center retrospective study and waived the requirement for informed patient consent.

Acknowledgements

This work was supported by a National Research Foundation (NRF) grant funded by the Korea government, Ministry of Science and ICT (MSIP, 2018R1A2B6009076).

References

[1] Z.S. Rosenberg, J. Beltran, J.T. Bencardino, From the RSNA refresher courses. Radiological Society of North America. MR imaging of the ankle and foot, Radiographics (2000) S153–S179.
[2] P. Holmer, L. Sondergaard, L. Konradsen, P.T. Nielsen, L.N. Jorgensen, Epidemiology of sprains in the lateral ankle and foot, Foot Ankle Int. 15 (2) (1994) 72–74.
[3] K.D. Harrington, Degenerative arthritis of the ankle secondary to long-standing lateral ligament instability, J. Bone Joint Surg. 61 (3) (1979) 354–361. American volume.
[4] V. Valderrabano, B. Hintermann, M. Horisberger, T.S. Fung, Ligamentous post-traumatic ankle osteoarthritis, Am. J. Sports Med. 34 (4) (2006) 612–620.
[5] P. Aerts, D.G. Disler, Abnormalities of the foot and ankle: MR imaging findings, AJR Am. J. Roentgenol. 165 (1) (1995) 119–124.
[6] K.J. Stevens, R.F. Busse, E. Han, A.C. Brau, P.J. Beatty, C.F. Beaulieu, G.E. Gold, Ankle: isotropic MR imaging with 3D-FSE-cube–initial experience in healthy volunteers, Radiology 249 (3) (2008) 1026–1033.
[7] M. Notohamiprodjo, B. Kuschel, A. Horng, D. Paul, P. Baer, G. Li, J.M. Garcia del Olmo, M.F. Reiser, C. Glaser, 3D-MRI of the ankle with optimized 3D-SPACE, Invest. Radiol. 47 (4) (2012) 231–239.
[8] J. Yi, J.G. Cha, Y.K. Lee, B.R. Lee, C.H. Jeon, MRI of the anterior talofibular ligament, talar cartilage and os subfibulare: comparison of isotropic resolution 3D and conventional 2D T2-weighted fast spin-echo sequences at 3.0 T, Skeletal Radiol. 45 (7) (2016) 899–908.
[9] H.J. Park, S.Y. Lee, N.H. Park, M.H. Rho, E.C. Chung, J.H. Park, S.J. Park, Three-dimensional isotropic T2-weighted fast spin-echo (VISTA) ankle MRI versus two-dimensional fast spin-echo T2-weighted sequences for the evaluation of anterior talofibular ligament injury, Clin. Radiol. 71 (4) (2016) 349–355.
[10] M. Kim, Y.S. Choi, M.S. Jeong, M. Park, T.J. Chun, J.S. Kim, K.W. Young, Comprehensive assessment of ankle syndesmosis injury using 3D isotropic Turbo spin-Echo sequences: diagnostic performance compared with that of conventional and oblique 3-T MRI, AJR Am. J. Roentgenol. 208 (4) (2017) 827–833.
[11] V. Kalia, B. Fritz, R. Johnson, W.D. Gilson, E. Raithel, J. Fritz, CAIPIRINHA accelerated SPACE enables 10-min isotropic 3D TSE MRI of the ankle for optimized visualization of curved and oblique ligaments and tendons, Eur. Radiol. 27 (9) (2017) 3652–3661.
[12] H.S. Kim, Y.C. Yoon, J.W. Kwon, B.K. Choe, Qualitative and quantitative assessment of isotropic ankle magnetic resonance imaging: three-dimensional isotropic intermediate-weighted turbo spin echo versus three-dimensional isotropic fast field echo sequences, Korean J. Radiol. 13 (4) (2012) 443–449.
[13] J.F. Glockner, H.H. Hu, D.W. Stanley, L. Angelos, K. King, Parallel MR Imaging: A User's Guide 1, Radiographics 25 (5) (2005) 1279–1297.
[14] H.J. Park, S.Y. Lee, N.H. Park, M.H. Rho, E.C. Chung, J.H. Park, S.J. Park, Three-dimensional isotropic T2-weighted fast spin-echo (VISTA) ankle MRI versus two-dimensional fast spin-echo T2-weighted sequences for the evaluation of anterior talofibular ligament injury, Clin. Radiol. (2016).
[15] M. Lustig, D. Donoho, J.M. Pauly, Sparse MRI: the application of compressed sensing for rapid MR imaging, Magn. Reson. Med. 58 (6) (2007) 1182–1195.
[16] S.S. Vasanawala, M.T. Alley, B.A. Hargreaves, R.A. Barth, J.M. Pauly, M. Lustig, Improved pediatric MR imaging with compressed sensing, Radiology 256 (2) (2010) 607–616.

[17] R. Kijowski, H. Rosas, A. Samsonov, K. King, R. Peters, F. Liu, Knee imaging: rapid three-dimensional fast spin-echo using compressed sensing, J. Magn. Reson. Imaging 45 (6) (2017) 1712–1722.
[18] N. Seo, M.S. Park, K. Han, D. Kim, K.F. King, J.Y. Choi, H. Kim, H.J. Kim, M. Lee, H. Bae, M.J. Kim, Feasibility of 3D navigator-triggered magnetic resonance cholangiopancreatography with combined parallel imaging and compressed sensing reconstruction at 3T, J. Magn. Reson. Imaging 46 (5) (2017) 1289–1297.
[19] F.F. Altahawi, K.J. Blount, N.P. Morley, E. Raithel, I.M. Omar, Comparing an accelerated 3D fast spin-echo sequence (CS-SPACE) for knee 3-T magnetic resonance imaging with traditional 3D fast spin-echo (SPACE) and routine 2D sequences, Skeletal Radiol. 46 (1) (2017) 7–15.
[20] S.H. Lee, Y.H. Lee, J.-S. Suh, Accelerating knee MR imaging: compressed sensing in isotropic three-dimensional fast spin-echo sequence, Magn. Reson. Imaging (2017).
[21] Z. Wang, A.C. Bovik, H.R. Sheikh, E.P. Simoncelli, Image quality assessment: from error visibility to structural similarity, IEEE Trans. Image Process. 13 (4) (2004) 600–612.
[22] K.G. Hollingsworth, D.M. Higgins, M. McCallum, L. Ward, A. Coombs, V. Straub, Investigating the quantitative fidelity of prospectively undersampled chemical shift imaging in muscular dystrophy with compressed sensing and parallel imaging reconstruction, Magn. Reson. Med. 72 (6) (2014) 1610–1619.
[23] M.S. Cohen, R.M. Weisskoff, Ultra-fast imaging, Magn. Reson. Imaging 9 (1) (1991) 1–37.
[24] J. Tsao, Ultrafast imaging: principles, pitfalls, solutions, and applications, J. Magn. Reson. Imaging 32 (2) (2010) 252–266.
[25] Q. Chen, K.W. Stock, P.V. Prasad, H. Hatabu, Fast magnetic resonance imaging techniques, Eur. J. Radiol. 29 (2) (1999) 90–100.
[26] F. Maspes, A. Apruzzese, E. Squillaci, R. Floris, P. Santino, G. Simonetti, [An introduction to fast and ultrafast sequences in magnetic resonance], La Radiologia medica 88 (3) (1994) 249–258.
[27] M. Kiss, P. Hermann, Z. Vidnyanszky, V. Gal, Reducing task-based fMRI scanning time using simultaneous multislice echo planar imaging, Neuroradiology 60 (3) (2018) 293–302.
[28] L. Tanenbaum, A. Tsiouris, A. Johnson, T. Naidich, M. DeLano, E. Melhem, P. Quarterman, S. Parameswaran, A. Shankaranarayanan, M. Goyen, Synthetic MRI for clinical neuroimaging: results of the magnetic resonance image compilation (MAGiC) prospective, multicenter, multireader trial, Am. J. Neuroradiol. 38 (6) (2017) 1103–1110.
[29] K.G. Hollingsworth, Reducing acquisition time in clinical MRI by data undersampling and compressed sensing reconstruction, Phys. Med. Biol. 60 (21) (2015) R297–322.
[30] P.W. Worters, K. Sung, K.J. Stevens, K.M. Koch, B.A. Hargreaves, Compressed-sensing multispectral imaging of the postoperative spine, J. Magn. Reson. Imaging 37 (1) (2013) 243–248.
[31] J.Y. You, G.Y. Lee, J.W. Lee, E. Lee, H.S. Kang, An osteochondral lesion of the distal tibia and fibula in patients with an osteochondral lesion of the talus on MRI: prevalence, location, and concomitant ligament and tendon injuries, AJR Am. J. Roentgenol. 206 (2) (2016) 366–372.
[32] I. Elias, S.M. Raikin, M.E. Schweitzer, M.P. Besser, W.B. Morrison, A.C. Zoga, Osteochondral lesions of the distal tibial plafond: localization and morphologic characteristics with an anatomical grid, Foot Ankle Int. 30 (6) (2009) 524–529.
[33] Y. Han, J. Yoo, H.H. Kim, H.J. Shin, K. Sung, J.C. Ye, Deep learning with domain adaptation for accelerated projection-reconstruction MR, Magn. Reson. Med. 80 (3) (2018) 1189–1205.
[34] J.A. de Zwart, P.J. Ledden, P. van Gelderen, J. Bodurka, R. Chu, J.H. Duyn, Signal-to-noise ratio and parallel imaging performance of a 16-channel receive-only brain coil array at 3.0 Tesla, Magn. Reson. Med. 51 (1) (2004) 22–26.
[35] M. Weiger, K.P. Pruessmann, C. Leussler, P. Roschmann, P. Boesiger, Specific coil design for SENSE: a six-element cardiac array, Magn. Reson. Med. 45 (3) (2001) 495–504.
[36] M. Buehrer, M.E. Huber, F. Wiesinger, P. Boesiger, S. Kozerke, Coil setup optimization for 2D-SENSE whole-heart coronary imaging, Magn. Reson. Med. 55 (2) (2006) 460–464.
[37] S.J. Erickson, R.W. Prost, M.E. Timins, The "magic angle" effect: background physics and clinical relevance, Radiology 188 (1) (1993) 23–25.